VTA neurons coordinate with the hippocampal reactivation of spatial experience

Stephen N Gomperts, Fabian Kloosterman, Matthew A Wilson

DOI: http://dx.doi.org/10.7554/eLife.05360

Cite as: eLife 2015;10.7554/eLife.05360

Received: 28 October 2014
Accepted: 13 October 2015
Published: 14 October 2015

VTA neurons coordinate with the hippocampal reactivation of spatial experience

Stephen N. Gomperts[1,2,3], Fabian Kloosterman[4,5,6], and Matthew A. Wilson[2,3]

1. MassGeneral Institute for Neurodegenerative Disease, Department of Neurology, Massachusetts General Hospital, Charlestown, Massachusetts
2. Department of Brain and Cognitive Sciences, Massachusetts Institute of Technology, Cambridge, Massachusetts
3. Picower Institute for Learning and Memory, Massachusetts Institute of Technology, Cambridge, Massachusetts
4. NERF, Leuven, Belgium
5. imec, Leuven, Belgium
6. Laboratory of Biological Psychology, Department of Psychology, KU Leuven, Leuven, Belgium

ABSTRACT

Spatial learning requires the hippocampus, and the replay of spatial sequences during hippocampal sharp wave-ripple (SPW-R) events of quiet wakefulness and sleep is believed to play a crucial role. To test whether the coordination of VTA reward prediction error signals with these replayed spatial sequences could contribute to this process, we recorded from neuronal ensembles of the hippocampus and VTA as rats performed appetitive spatial tasks and subsequently slept. We found that many reward responsive (RR) VTA neurons coordinated with quiet wakefulness-associated hippocampal SPW-R events that replayed recent experience. In contrast, coordination between RR neurons and SPW-R events in subsequent slow wave sleep was diminished. Together, these results indicate distinct contributions of VTA reinforcement activity associated with hippocampal spatial replay to the processing of wake and SWS-associated spatial memory.

Introduction

Hippocampal dependent learning and memory formation are influenced by reward and are believed to occur during distinct behavioral states. As animals explore the environment, hippocampal place cells fire sequentially under the modulation of the theta rhythm. Subsequently, these sequences of neuronal activity are replayed in association with hippocampal sharp wave-ripple (SPW-R) events of quiet wakefulness and sleep[1,2,3,4]. SPW-R events contribute to spatial learning[5,6,7], and the capacity for reward to influence reactivation of CA3 place cell pairs in SPW-R events[8] suggests that reward-related neural activity is likely to play an important role in this process. It has been

unclear whether replay events of quiet wakefulness and sleep differ in their contribution to learning and memory, but the observation that replay events during slow wave sleep (SWS) are lower fidelity than replay events during quiet wakefulness[9] supports this possibility.

Dopamine neurons of the VTA represent reward prediction error[10] and appear to be an important brain substrate for reinforcement learning[11]. Optogenetic activation of dopamine cells during spatial learning has recently been demonstrated to increase the reactivation of CA1 place cell pairs in sleep and stabilize subsequent spatial learning[12]. In addition, electrical stimulation of the medial forebrain bundle triggered on a hippocampal place cell's spikes has recently been shown to drive goal-directed behavior toward its place field[13]. However, it is unclear how under normal physiological conditions dopamine neuronal activity engages with the hippocampus. Dopamine cells could coordinate with and reinforce replayed hippocampal sequences. In addition, the fast-onset, slowly decaying profile of dopamine synaptic release has led to the suggestion that dopamine could implement the propagation of expected value across reactivated hippocampal sequences[3]. We hypothesized that replayed hippocampal spatial sequences would coordinate with reward-related representations of VTA neurons during tasks that place demands on spatial memory. Here, we acquired simultaneous multi-electrode (tetrode) recordings of neurons of the hippocampus and the VTA as rats performed appetitive spatial tasks and subsequently slept to determine the relationship between VTA neuronal activity, hippocampal SPW-R-associated activity, and sequence replay. We show that many reward responsive (RR) VTA neurons modulate their firing rate with

SPW-R events of quiet wakefulness. Modulation of VTA unit activity was greater in SPW-R events associated with hippocampal replay of task-associated sequences. In contrast to nonRR VTA unit activity, RR unit activity preferentially coordinated with replayed representations of reward sites. In addition, RR VTA units more strongly phase-locked to the hippocampal theta rhythm than nonRR units, and RR VTA units that more strongly coupled to hippocampal theta had greater coordination with replayed reward site representations. In contrast to these findings in the awake state, in post-task epochs of SWS, SPW-R modulation of RR VTA unit activity was significantly reduced. Furthermore, within SWS, RR unit activity decreased during periods of hippocampal SPW-R reactivation. Together, these results indicate distinct contributions of VTA reinforcement activity associated with hippocampal spatial replay to the processing of wake and SWS-associated spatial memory.

Results

Coordination of VTA unit activity with hippocampal SPW-R events of quiet wakefulness

We recorded the activity of multiple simultaneously isolated units of the hippocampus (499 total; for each recording, median of 25, range 12-37) and VTA (84 total; median of 5, range 2 - 9) in five animals, as animals performed a spatial working memory (SWM) task[14] (three rats) (**Figure 1A**) or ran on a linear track (two rats) for food reward. The latter task was selected both because the observation of awake replay has been best characterized in a linear environment and because it provides a choice-free spatial task for contrast. Many VTA units modified their firing rate during goal approach and with

acquisition of food rewards (n=47/84), consistent with prior observations[15,16,17] (**Figure 1B; Materials and Methods)**. These results have been interpreted as the representation of reward prediction error in instrumental tasks[15,16,17] (specifically, the Q-associated temporal difference prediction error, where Q-value is the value of selecting a particular action at a given state) . The mean firing rates for reward responsive (RR) and non-reward responsive (nonRR) VTA units were 6.61±1.33 Hz (mean±s.e.m., RR units, n=47) and 20.59±5.49 Hz (nonRR units, n=24), respectively**)**. Two populations of cells were observed in a plot of waveform duration versus trough to peak ratio, consistent with prior reports[18] (**Figure 1C**). Most RR cells (38/47) fell in the longer duration cluster (> 1 ms), which appears to be enriched for putative dopamine cells[18,19].

SPW-R events, identified using hippocampal multiunit activity and local field potential (see **Materials and Methods**), were prominent at reward sites during pauses in run behavior between trials (**Figure 2AB**) and were measured in the period between nosepoke and run initiation to the next reward site. Reward acquisition occurred within the first 1 second of nosepoke. Reward site dwell times were variable and self-paced, with a median of 9.3 s (range: 1.5 s to 615.0 s). The frequency of SPW-R events on the SWM task was higher during pauses at reward locations on correct (rewarded) trials than on error trials (correct: 0.088±0.019 Hz; error: 0.029±0.009 Hz; $p<0.01$, signed-rank test), consistent with prior results[8].

Many (20/84) VTA units significantly modulated their firing around SPW-R events ($p<0.05$, bootstrapped confidence intervals; median baseline-normalized modulation

amplitude of 0.15; range 0.0003-1.41; n=84; **Figure 2**). Both positive and negative SPW-R modulations were observed (positive n=13; negative n=7; **Figure 2- figure supplement 1**). Most SPW-R modulations coincided with SPW-R events; however, some negative SPW-R modulations occurred on a longer timescale, flanking SPW-R events.

The majority of VTA units that were significantly modulated at SPW-R events were RR (17/20 compared to 47/84 recorded, p=0.03, chi = 4.6, Chi-square test), and SPW-R modulation depth was greater for RR units than nonRR units (RR units 0.21±0.04, n=45; nonRR units 0.11±0.02; p=0.017, n=23, rank-sum test). For RR units, the sign of SPW-R modulation correlated with the sign of firing rate changes associated with reward acquisition (r=0.55, p=1.2x10^{-4}). Modulation of RR units at SPW-R events did not require active reward consumption, as a similar modulation depth (0.26±0.05) was noted when only SPW-R events delayed relative to nosepoke by at least 6 seconds were considered (signed-rank test, p=0.7). SPW-R modulation depth for RR VTA units was not significantly different on the SWM task compared to the linear track (SWM task, 0.26±0.06, n=26; linear track, 0.13±0.02, n=19, p=0.3, rank-sum test).

We next sought to determine whether RR unit modulation around SPW-R events was related to hippocampal replay. To evaluate spatial information associated with SPW-R replay events, we used a clusterless, probabilistic reconstruction method to maximize decoding fidelity[20]. First, we confirmed that the recorded hippocampal neuronal population conveyed sufficient spatial information to accurately decode the rat's position

on the track. Indeed, a cross-validation procedure showed that decoded hippocampal activity accurately reflected the rat's location during run behavior (speed > 10 cm/s), with median error of 8.3±0.5 cm across recording sessions (**Figure 3- figure supplement 1A-C**; see **Materials and Methods**). We also confirmed that this clusterless reconstruction method resulted in lower median error than a cluster-based approach (median error 15.2±1.9 cm, $p=1.22\times10^{-4}$, signed-rank test, n=14 recordings).

Reconstruction of hippocampal activity during pauses in run behavior (speed < 10 cm/s; in 25 ms time bins) identified putative replay events: the representation of a sequence of locations during SPW-R events (**Figure 3- figure supplement 1D**). For each event, we computed the statistical likelihood that the decoded positions represented a constant-speed traversal of a trajectory on the track[21,22] and compared it to distributions obtained after two separate randomization procedures (see **Materials and Methods**). Replay events identified with this approach constituted 24.8±2% (1107/4645) of SPW-R events.

Modulation of RR VTA unit activity was greater in SPW-R events associated with replay of sequential experience of the task than in SPW-R events that were not (modulation depth 0.28±0.04 vs. 0.15±0.03, $p=4.5\times10^{-4}$, signed-rank test; n=40; **Figure 3**). In contrast, for nonRR VTA units, modulation depth was similar across replay and nonreplay events (replay 0.11±0.02; nonreplay 0.11±0.03; $p=0.6$; signed-rank test; n=22).

We sought to determine whether the greater modulation of RR units around replay-associated SPW-R events compared to nonreplay-associated SPW-R events derived from some difference other than sequence replay. Ripple power and peak hippocampal firing rate at replay and non-replay SPW-R events were not significantly different (p=0.6, p=1, respectively, signed-rank tests; **Figure 3- figure supplement 2A,B**). Replay events had longer durations than non-replay events (0.209±0.003 s vs. 0.161±0.002 s, $p<5.0\times10^{-16}$, rank-sum test). To address whether SPW-R event duration alone could drive modulation of RR VTA unit activity, we constructed a dataset of replay and nonreplay events matched on their range of durations. Across these matched groups, the greater modulation of RR units at replay events compared to nonreplay events was preserved (replay 0.33±0.05; nonreplay 0.24±0.05, p=0.01, signed-rank test). Similarly, RR units at non-replay events separated by median split into short (100.6±0.0 ms) and long (222.6±0.1 ms) events had similar degrees of modulation (modulation depth of short events 0.20±0.04; long events 0.17±0.03; p=0.9, signed-rank test; n=40 RR units); and RR units at replay events split on median duration also did not differ in their modulation depth (short events 0.29±0.04; long events 0.39±0.06; p=0.2, signed-rank test).

Despite these similarities, replay events and nonreplay events differed with respect to the fraction of isolated pyramidal units active during each SPW-R event (replay 35.6±0.0%; nonreplay 28.7±0.0%, p=0.001, signed-rank test; n=14 recordings) and with respect to the number of single unit action potentials per unit present in each burst (replay 1.06±0.07; nonreplay 0.72±0.09; $p=6.1\times10^{-4}$, signed-rank test). To address whether the greater activation of RR units around the time of replay events could be due to the greater

intensity of hippocampal pyramidal cell spiking seen during these events, we constructed a dataset of spike count matched replay and non-replay events. Across the spike count matched groups, the greater modulation of RR units at replay events compared to nonreplay events was maintained (replay 0.28±0.04; nonreplay 0.19±0.03, p=0.03, sign rank test). Thus, the greater modulation depth of RR units at replay events compared to nonreplay events did not derive from differences in the intensity of hippocampal spiking.

We next evaluated whether the difference in RR unit coordination with replay and nonreplay events arose from differences in the timing of these events in the immediate post-reward period, when the activity of RR units often changes. Replay and nonreplay events occurring within a 5 second window from the nosepoke had similar onset latencies (replay events 2.54±0.10 s, n=130; nonreplay events 2.67±0.07 s, n=217, p=0.3, rank-sum test), and the temporal distributions of replay and nonreplay events following reward delivery were similar (p=0.2, Kolmogorov-Smirnov test; **Figure 3- figure supplement 2C**). These data suggest that RR units coordinate preferentially with hippocampal SPW-R events that encode within-session spatial sequences.

Engagement of VTA unit activity with replayed spatial content

The coordination of a reward prediction error signal with a hippocampal replay sequence (for example, one that represents a trajectory towards a reward) could function to reinforce specific elements of the reactivated sequence, such as a goal location. We therefore explored how VTA unit activity relates to the specific spatial locations contained in replay content. To account for latency between hippocampal SPW-R events

and VTA activity, we first examined the hippocampal SPW-R event-triggered VTA LFP. This revealed a prominent negative potential that peaked 84±13 ms after SPW-R onset (**Figure 4A**). We focused on replay events occurring at forced reward locations, which represent the beginning of choice trials and which comprised the majority of replay events (703/876, 80.3%; compared to 173 at choice reward locations). For each recording, we constructed a distribution of all decoded locations within these replay events and compared this to the distribution of decoded spatial locations specifically associated with 84 ms delayed RR VTA unit spikes and nonRR VTA unit spikes.

Across replay events, the probability of decoded spatial locations was biased toward reward sites (probability/spatial bin of replay content at reward locations 0.038±0.005 bin^{-1}; non-reward locations 0.021±0.002 bin^{-1}; $p=2.4\times10^{-4}$, signed-rank test; n=14 recording sessions; see **Materials and Methods**; **Figure 4C**). Incorporating the latency of 84 ms, the timing of RR VTA unit activity within replay events specifically coincided with the replay of reward locations (probability/spatial bin of VTA unit activity at reward locations 0.044±0.003 bin^{-1}; non-reward locations 0.021±0.001 bin^{-1}; $p=9.0\times10^{-8}$ signed-rank test; n=41 RR units). Across all recordings, RR VTA unit spikes were biased to coincide with replayed reward site locations in excess of the proportion of reward site locations within replay events (reward site bias for replay events: 0.451±0.007; excess reward site bias for RR VTA units: 0.022±0.011 (mean±s.d.); $p=0.048$, chi = 3.9, Chi-square test; see **Materials and Methods**; **Figure 4B,D**). In contrast, nonRR units did not preferentially coordinate with replayed reward site locations (excess reward site bias for nonRR VTA units: -0.013±0.010; $p=0.3$, chi=1.2, Chi-square test; **Figure 4B,E**). The

contrast of excess reward site bias of RR units and nonRR units was significant ($p<0.016$, nonparametric permutation test; see **Materials and Methods**). The bias in coordination of RR units but not nonRR units with replayed reward locations persisted when the current location of the animal was excluded from the analysis (reward site bias for replay events: 0.331±0.009; excess reward site bias for RR VTA units: 0.031±0.014; p=0.041 chi = 4.2 Chi-square test; nonRR VTA units: 0.008±0.013; p=0.6, chi=0.2, Chi-square test). These data suggest that RR VTA units preferentially associate with the hippocampal replayed representation of reward locations.

To evaluate the task dependence of this observation, we compared the preferential coordination of RR units with replayed reward site locations on the SWM task and on the linear track. Interestingly, the excess reward site bias of RR units was greater on the SWM task than on the linear track (excess reward site bias for RR units on the SWM task 0.027±0.014; excess reward site bias for RR units on the linear track 0.017±0.015; p=0.045, nonparametric permutation test). Because this task-dependence could reflect a role for the coordination of RR units with replayed reward locations in choice behavior, we examined whether the preferential coordination of RR units with replayed reward site locations reflected recent choice behavior or predicted future choice behavior on the SWM task. However, we were unable to detect a difference in the excess reward site bias of RR units at replay events immediately following correct trials versus error trials (excess reward site bias after correct trials 0.022±0.020; after error trials -0.018±0.031; p=0.19, nonparametric permutation test). Similarly, the excess reward site bias of RR units at replay events was no greater immediately prior to correct trials than prior to error

trials (excess reward site bias prior to correct trials 0.001±0.021; prior to error trials 0.013±0.041, p=0.6, nonparametric permutation test). These results suggest that the preferential coordination of RR unit activity with replayed reward locations is task dependent but may not simply recapitulate or predict immediate reward-associated experience.

Coordination of VTA units with specific replayed spatial sequences

Previous work has posited a specific coordination between dopamine neuronal activity and replay events comprised of spatial sequences starting locally and replaying away from the animal (centrifugal events) in reverse order compared to their order during behavior[3]. To address whether the preferential coordination of RR VTA units with replayed reward site locations may derive from a selective engagement of VTA units with centrifugal replay events or with reverse replay events, in distinction from replay sequences that start remotely and replay towards the animal (centripetal events), or forward replay sequences that replay in the same order as they did during behavior, we first differentiated between instantaneous centrifugal and centripetal spatial content, and between forward and reverse spatial content, by reconstructing SPW-R replay events at forced reward sites using both position and run direction data (**Figure 5A-C**; see **Materials and Methods**). We accumulated centrifugal, centripetal, forward, and reverse replayed spatial distributions separately, and we compared them to each other and to the distribution of decoded spatial locations and run direction specifically associated with RR VTA unit spikes.

RR units preferentially coordinated with the reward site representation of centrifugal replay events but not centripetal replay events (reward site bias for centrifugal replay spatial content 0.493±0.005; excess reward site bias for RR units at centrifugal replay 0.051±0.020; p=0.014, chi=6.0, Chi-square test; reward site bias for centripetal replay spatial content 0.524±0.006; excess reward site bias for RR units at centripetal replay 0.016±0.021; p=0.5, chi=0.5, Chi-square test; **Figure 5D,E**). In contrast, nonRR units showed no excess reward site bias for replayed spatial content (excess reward site bias for nonRR units at centrifugal replay 0.002±0.019, p=1, chi=0.001, Chi-square test; at centripetal replay: 0.011±0.022; p=0.6, chi=0.2). These results demonstrate that RR units preferentially coordinate with centrifugal replay content.

We next examined RR and nonRR unit activity associated with forward and reverse replay events. The probability of decoding spatial locations at reward sites was similar for forward and reverse replay events (reward site bias for forward replay spatial content 0.422±0.013; reward site bias for reverse replay spatial content 0.419±0.014; p=0.9, chi=0.2, Chi-square test). We did not detect a selective engagement of RR units with reward locations of reverse replay over forward replay (excess reward site bias for RR units at reverse replay 0.035±0.020; at forward replay 0.034±0.020; p=1, nonparametric permutation test).

To evaluate the task dependence of the preferential coordination of VTA RR units with centrifugal replay spatial content, we analyzed the SWM task and the linear track separately. Similar to the results described above, RR units acquired on the SWM task

preferentially coordinated with reward site representations of centrifugal replay events (excess reward site bias for RR units at centrifugal replay: 0.071±0.032; p=0.028, chi=4.8) in contrast to centripetal replay events (excess reward site bias for RR units at centripetal replay: 0.031±0.028 p=0.3, chi=1.0; **Figure 5- figure supplement 1**). However, this preferential coordination was not observed on the linear track (excess reward site bias for RR units at centrifugal replay on the linear track: 0.040±0.024; p=0.11, chi=2.5; excess reward site bias for RR units at centripetal replay: -0.004±0.031; p=0.9, chi=0.01). Thus, the coordination of VTA RR units with centrifugal replay of reward site locations was stronger on the SWM task.

Phase-locking of VTA units to hippocampal theta during run behavior correlates with the engagement of VTA units with replayed spatial content

In addition to modulating their activity at hippocampal SPW-R events, many VTA units (39/84; 43%) phase-locked to hippocampal theta during run behavior (Rayleigh test for uniformity against unimodal alternative $p < 0.05$, phase preference -10±16 degrees, relative to the peak of theta), consistent with previous observations[18] **(Figure 6)**. The coordination of neural activity with the hippocampal theta rhythm has been proposed to be a mechanism used in spatial working memory[14,18]. We therefore sought to determine the extent to which theta phase-locking of VTA units predicted their coordination with SPW-R events. Circular concentration of VTA unit spikes around the mean preferred hippocampal theta phase was greater for RR units than nonRR units, as measured with the circular concentration coefficient kappa as described previously[14,23], (mean±s.e.m., RR: 0.139±0.012, n=47; nonRR: 0.099±0.019, n=24; p=0.03, rank-sum test; **Figure 6B**).

For theta-modulated RR units but not theta-modulated nonRR units, circular concentration at hippocampal theta positively correlated with the probability that spike-associated replayed spatial content represented reward locations (RR units: r=0.51, p=0.04, n=17; nonRR units: r=0.45, p=0.13, n=13; **Figure 6C**). In contrast, the circular concentration coefficient of VTA units at hippocampal theta did not correlate with the firing rate of those units (RR units: r=-0.22, p=0.4, n=18; nonRR units: r=-0.49, p=0.09, n=13). In addition, the circular concentration of RR units at hippocampal theta did not correlate with their modulation depth at SPW-R replay events (r=0.12, p=0.5, n=45). Thus, phase-locking of RR units to hippocampal theta during run behavior was associated with the timing but not the number of spikes of RR units at SPW-R events.

Coordination between VTA unit activity and hippocampal SPW-R events in slow wave sleep

Previous work has demonstrated hippocampal SPW-R replay during SWS [2,24-27] and has shown that medial forebrain bundle stimulation triggered on place cell activity in sleep exerts a powerful influence on post-sleep behavior[13]. Having identified replay-related modulation of VTA unit activity, we therefore sought to evaluate SPW-R-associated VTA unit activity in SWS acquired immediately subsequent to run behavior.

Both RR and nonRR VTA units reduced their firing rates in SWS (RR units: run 8.8±1.7 Hz, quiet wakefulness 6.6±1.3 Hz, SWS 4.5±0.8 Hz; run vs SWS, $p=2.2\times10^{-7}$; quiet vs SWS, $p=2.3\times10^{-5}$; signed-rank tests, n=47; nonRR units: run 26.8±7.2 Hz, quiet wakefulness 20.6±5.4 Hz, SWS 10.4±2.7 Hz; run vs SWS, $p=7.1\times10^{-5}$; quiet vs SWS,

$p=1.0\times10^{-4}$; signed-rank tests, n=24). In addition, the modulation depth of RR unit activity at SPW-R events was significantly reduced in SWS (modulation depth in quiet wakefulness 0.21±0.04; in SWS 0.10±0.02; p=0.003, rank-sum test, n=45 in quiet wakefulness, n=39 in SWS; **Figure 7A-C**). In contrast to the awake state, RR units in SWS were often negatively modulated at SPW-R events (30/39 units, p= 0.001, sign test). Modulation depths in quiet wakefulness and sleep were significantly correlated (modulation depth, r=0.47, p=0.002, n=39), but the sign of modulation across these states was not (modulation sign, r=0.13, p=0.4, n=39). In contrast to RR units, the SPW-R modulation of nonRR units was not significantly modified by behavioral state (modulation depth in quiet wakefulness 0.11±0.02; SWS 0.06±0.01; p=0.13, rank-sum test, n=23 in quiet wakefulness, n=20 in SWS; **Figure 7C**). Thus, RR units coordinated more robustly with hippocampal SPW-R events of quiet wakefulness than with those of SWS.

The smaller modulation of RR units with SPW-R events in SWS compared to quiet wakefulness could result from a difference in state or from a difference in the spatial content expressed in these states. For example, replayed spatial content in sleep may be less biased by recent experience than replayed spatial content in quiet wakefulness. To explore this question, we set out to examine hippocampal replay in detail in SWS.

We first evaluated the prevalence of replay-associated SPW-R events in SWS. Hippocampal replay of recent experience during SWS identified using Bayesian position reconstruction was less prevalent than during quiet wakefulness (SWS 16.0±1.7%

(800/5820), compared with 24.8±2% of wake-associated SPW-R events, p=0.003, signed-rank test).

Hippocampal activity in SWS is characterized by epochs of up-state-like neuronal population activity known as frames, within which SPW-R events occur and during which coordinated replay between the hippocampus and neocortex has been observed[27]. Because hippocampal replay in SWS has been associated with SPW-R events within frames, we compared VTA unit activity across frames associated with high versus low SPW-R rates (SPW-R events per second), relative to the mean. RR unit firing rate was lower in high rate SPW-R frames than in low rate SPW-R frames (high rate SPW-R frames 4.23±0.74 Hz; low rate SPW-R frames 4.64±0.77 Hz; signed-rank test, p=0.003, n=47; **Figure 7D-H**). In contrast, nonRR unit firing rate was similar across these groups of frames (high rate SPW-R frames 10.26±2.66 Hz; low rate SPW-R frames 10.41±2.65 Hz; signed-rank test, p=0.45, n=24; **Figure 7D-H**). Thus, RR unit activity was biased away from SPW-R rich frames.

We next asked whether VTA unit firing rates varied with frame-associated replay of recent experience. For this purpose, we evaluated average spatial content in each frame, measured as the average across time bins of the maximum decoded probability at each time bin. RR unit firing rate was lower in frames associated with higher spatial content (above the mean spatial content of frames) than in frames associated with lower spatial content (below the mean; RR unit firing rate at high spatial content frames 4.11±0.78 Hz vs. firing rate at low spatial content frames 4.83±0.91 Hz, p=0.001; signed-rank test,

n=42). Frames with higher spatial content were longer than frames with lower spatial content (median 3.98 s vs. 1.85 s; p=0.009; signed-rank test, n=14 recordings). Because differences in frame duration could affect estimates of within-frame firing rates, we also performed an inverse analysis, in which we sorted hippocampal frames by the associated firing rate of VTA units and then compared their spatial content associated with recent experience. Frames associated with high RR unit firing rate (above the mean firing rate for each unit) had lower mean spatial content than frames associated with low (below the mean) RR unit firing rate (spatial content at high firing rate frames 0.185±0.012 (a.u.) vs. spatial content at low firing rate frames 0.191±0.013 (a.u.); signed-rank test, p=0.045, n=42; **Figure 7I**). Together, these results demonstrate that SWS is associated with reduced SPW-R modulation of RR unit activity and with reduced RR unit activity in hippocampal frames containing a high rate of SPW-R events and in frames associated with high spatial information about recently explored environments.

Discussion

Hippocampal dependent learning and memory are influenced by reward, and SPW-R events contribute to these functions[5,6,7]. As VTA dopamine cells are driven by reward prediction errors[10] and have been suggested to provide an error signal to guide learning in downstream brain regions[11], we posited that the coincidence of dopamine neuronal activity with sequence replay in SPW-R events of quiet wakefulness could reinforce spatial experience, mediating the influence of reward on hippocampal dependent processing[8] and memory formation.

406 Taken collectively, the results of this study support this possibility, demonstrating that
407 during quiet wakefulness but not SWS, RR VTA neurons coordinate selectively with
408 hippocampal replay sequences and are biased in their timing towards the reactivated
409 representation of rewarded locations. In contrast, nonRR VTA neurons did not
410 coordinate with the specific spatial content of replay sequences. RR neurons were also
411 more strongly phase-locked to hippocampal theta than nonRR neurons, and the extent of
412 phase-locking correlated with the coordination of RR unit activity with replayed reward
413 locations. Previous work has demonstrated theta phase-dependent interactions between
414 the hippocampus, prefrontal cortex, and VTA during working memory-dependent, single
415 trial decisions[14,18]. Our data support a model in which these experience-dependent
416 associations, once established, are re-expressed in SPW-Rs of quiet wakefulness, to guide
417 spatial memory across trials. In addition, our results identify two possible endogenous
418 substrates by which optogenetically released dopamine can increase off-line reactivation
419 of hippocampal cells and improve spatial memory performance[12]: direct coordination of
420 dopamine neuronal activity with hippocampal replay of quiet wakefulness, or
421 coordination with hippocampal theta triggering a subsequent reactivation of dopamine
422 neurons that engages with hippocampal replay.
423
424 The sign of SPW-R modulation varied across RR neurons, often recapitulating their
425 reward-associated modulation of firing rate. This result suggests that as a population, RR
426 neurons replay their reward-related activity in concert with hippocampal sequence replay,
427 to selectively reinforce reward-associated behavior. Coordination with replay has
428 previously been observed in neurons of the primary visual cortex[27] and the striatum[28,29], a

429 major target of the VTA that represents rewards[30,31]. The current results extend these
430 findings, supporting the hypothesis that replay events engage both cortical and
431 subcortical structures to create an accurate memory trace of recent experience.
432
433 In this study, RR neurons preferentially coordinated with SPW-R events of quiet
434 wakefulness compared to SWS and were least active in SWS frames associated with high
435 spatial content. Although we observed a higher proportion of replay events in quiet
436 wakefulness than in SWS, consistent with prior observations[9], differences in the
437 prevalence of replay events in quiet wakefulness and SWS are unlikely to underlie the
438 impact of SWS on VTA activity, given that SWS frames with higher spatial content were
439 associated with greater reduction in RR unit activity. These results suggest a functional
440 distinction between brain processes that subserve spatial memory within sessions versus
441 spatial learning across sessions, consistent with prior observations that tie awake
442 hippocampal replay events to within-session performance[5] yet associate replay events in
443 post-session epochs rich in SWS to cross-session spatial learning[6,7].
444
445 Memory consolidation in SWS is likely to require broad evaluation of behavioral
446 experiences, and the present results suggest that this evaluation can occur in the absence
447 of their reward prediction contingencies, as represented in the activity of VTA neurons.
448 In this regard, introducing anomalous reward prediction-related activity during sleep via
449 medial forebrain bundle stimulation triggered on place cell activity[13] has been recently
450 demonstrated to drive goal-directed spatial behavior in wakefulness. In neuropsychiatric

diseases such as addiction or obsessive compulsive disorders, such anomalous associations could contribute to maladaptive behaviors.

In contrast to the state-dependence of VTA-hippocampal interactions, neurons of the ventral striatum have been found to coordinate with hippocampal replay in SWS[28,29]. One possible explanation for this distinction, consistent with the suggested role of dopamine as a teaching signal, is that VTA dopamine activity stabilizes and links replayed sequences in quiet wakefulness across brain regions for subsequent consolidative processes in SWS.

It is notable that replay events in these recordings were biased in their spatial content towards reward sites. The basis for this bias remains to be determined and may be driven by a number of factors not examined here, including the presence or expectation of reward, as well as differences in the dwell times, behavioral states, and behavioral repertoires manifested at reward and nonreward locations.

In this study, we observed a preferential engagement of RR units with the reward representation of centrifugal compared to centripetal replayed spatial content, while we did not detect a preference for RR units for the reward representation of reverse compared to forward replayed spatial content. These results are broadly consistent with the previous proposal that dopamine may function to propagate expected value across reactivated hippocampal sequences[3].

We also observed greater coordination of RR cells with replayed reward locations in the SWM task compared to the linear track, raising the possibility that VTA-hippocampal coordination at SPW-R events may reflect task contingencies. However, this result should be considered with caution given the limited sample size acquired in each task. Although we did not detect the preferential coordination of RR cells with replayed reward locations immediately after or immediately prior to successful choice behavior, as compared with errors, it remains possible that RR unit coordination with replayed reward locations could reflect (or predict) choice behavior on longer timescales. Of note, the experimental design was not intended to dissect the relationship of other task dependent features, such as uncertainty, to hippocampal-VTA coordination, and this will be worth pursuing in future experiments.

Interestingly, we found clear differences between RR neurons and nonRR neurons in their engagement with the hippocampus. A higher proportion of SPW-R modulated neurons were RR, RR neurons were more biased to fire in relation to replayed reward locations, and RR neurons demonstrated stronger phase-locking to the hippocampal theta rhythm. These results suggest that RR and nonRR neurons represent distinct functional classes of cells, perhaps associated with different cell types[32-35], that differentially contribute to hippocampal-dependent spatial memory. Given the uncertainty in the confidence with which dopamine cells can be identified on the basis of electrophysiologic criteria[19,32,36], however, we chose not to restrict our analysis to putative dopamine cells. Even so, over 80% of RR neurons had waveform properties that have been associated with dopamine cells, including a wide action potential and firing rates below 10 Hz.

Models of reinforcement learning have suggested distinct contributions of dopamine to certain forms of learning[37,38]. The specific, wake-associated coordination of RR VTA neurons with hippocampal activity may mediate the capacity for task-associated replay content to predict future paths to goal locations[39,13] and may underlie dopamine's stabilization of hippocampal replay[12]. These specific VTA-hippocampal interactions are likely to play a critical role in context-dependent reward seeking behavior. In addition, the state-dependent coordination of VTA reinforcement activity with hippocampal spatial replay events directs attention to the differential processing of spatial memory in wakefulness and SWS.

Materials and methods

All procedures were approved by the Committee on Animal Care of Massachusetts Institute of Technology and followed the ethical guidelines of the US National Institutes of Health.

Tetrode Implantation and recording

Five male Long-Evans rats (4-6 months old) were implanted under anesthesia (induction: ketamine (50 mg/kg) and xylazine (6 mg/kg); maintenance: isoflurane 0.5-3%,) with 2 arrays of independently movable recording tetrodes (for detailed methods, see reference 14). One array of 6-10 tetrodes was directed to the dorsal CA1 pyramidal cell layer (anterior-posterior (AP) -3.6 mm, lateral (L) +2.4 mm; relative to Bregma). A reference electrode was placed in the white matter above the hippocampal cell layer for differential

recordings. An additional array of 8-11 tetrodes was targeted to the VTA (AP -5.3 mm, L +1.0 mm). A tetrode without unit activity served as the local reference for VTA differential recordings. In one rat, stereotrodes as well as tetrodes were used for VTA recordings. Tetrodes were advanced to their target positions over several weeks. In 4 animals, an additional array of 4-8 electrodes was targeted to the prefrontal cortex for purposes unrelated to the present study. VTA tetrodes were lowered after each recording session and final electrode positions were confirmed with electrolytic lesions and histology[40] after recording was completed (**Figure 8**).

For hippocampal recording, 1 ms windows around thresholded extracellular action potentials were acquired on-line at 31 kHz, 300-6,000 Hz filtering. In order to retain wave-shape information for VTA units, which often have long waveforms, VTA unit recordings were acquired continuously at 31 kHz, 300-6,000 Hz filtering; and subsequently thresholded (60 μV) offline to isolate extracellular action potentials. Local field potentials (2 kHz sampling, 1-475 Hz filtering) were recorded from one electrode on each tetrode.

Head position and direction were monitored using overhead camera tracking of two sets of infrared diodes that were mounted on the headstage and that alternated at 30 Hz each.

Behavioral training

Animals were trained over 2-4 weeks to run a spatial appetitive choice task[14] on an end-to-end T-maze (**Figure 1**). Each trial consisted of two phases. In the sample phase, rats

were directed pseudorandomly to either the left (or right) reward site on the forced side of the maze, where a nosepoke-triggered grain pellet reward could be obtained (MedAssociates; Bioserv). In the test phase of the trial, rats traversed the central arm to a choice point, where they chose to go right (or left) in order to win reward on the choice side of the maze. The reward contingency was set up such that if the rat had been forced to turn left in the sample phase, then the correct response in the test phase was to turn right. Individual trajectories between reward sites on forced and choice sides were 300 cm long. After training, the animals were implanted with tetrode arrays. Following recovery from surgery, animals were food deprived to 85% of their free-feeding weights. Animals relearned the task slowly, improving from 60±3% (mean±s.e.m.) performance in the first three days of behavior to 74±2% in the final three behavioral sessions. Recordings on the spatial alternation task were acquired during the day over 22 days. Two animals ran only on a 200 cm linear track, to acquire food reward at both ends. Sleep sessions were acquired immediately after behavioral sessions in a sleep chamber with opaque walls within the recording room. Animals were housed in individual cages with a 12h light-12h dark standard light cycle.

Data analysis

Established software was used for initial identification and characterization of unit activity. This includes identification of well-isolated clusters of spike waveforms and differentiation of putative hippocampal pyramidal cells, hippocampal interneurons, and VTA units (Xclust, M. Wilson). Matlab (MathWorks, Natick, Massachusetts) was used

565 for further data analysis (https://github.com/stephengomperts/eLife_2015). Unless
566 otherwise stated, error bars reflect s.e.m.
567
568 Reward responsive (RR) VTA units in the SWM task were identified as those with
569 significantly different firing rates on correct versus error trials during approach to reward
570 (defined as the 2 second window prior to nosepoke) or reward acquisition (defined as the
571 3 second window following nosepoke; two-sided t-tests, $p<0.05$ for significance, n=27).
572 Reward responsiveness on the linear maze was determined by comparing firing rates
573 during reward acquisition to a 3 second window that ended 2 seconds before nosepoke.
574 These two approaches were highly correlated for the SWM task ($r=0.49$, $p=2.4\times10^{-4}$,
575 n=51). Differential VTA unit activity on correct versus error trials was common in our
576 dataset and is consistent with prior reports in instrumental tasks[15,16,17]. Such results have
577 been interpreted as the representation of choice-associated reward prediction error,
578 formalized for example in the Q-value associated temporal difference prediction error,
579 where Q-value is the value of selecting a particular action at a given state[15].
580
581 Waveform duration (time from peak to peak) and trough to peak ratio
582 (trough/(peak+trough)) were noted to distinguish two VTA unit populations, as shown
583 previously[18] (**Figure 1C**). Waveform duration and the biphasic duration[19] were highly
584 correlated ($r=0.79$, $p=8.53\times10^{-20}$, n=145).
585
586 Of 145 VTA units recorded, 84 units (47 RR; 24 nonRR; 13 unclassified due to low
587 firing rate (<0.3Hz)) were recorded concurrent with wake-associated hippocampal

588 activity, over 16 behavioral sessions in 5 rats, with 10 (2, 3, and 5) sessions on the end-
589 to-end T maze; 6 (4 and 2) sessions on the linear track, and in subsequent slow wave
590 sleep. Hippocampal activity in the 5th rat, acquired in 2 sessions on the linear track, was
591 insufficient for position reconstruction and assessment of hippocampal frames, reducing
592 the number of VTA units for replay and frame analyses to 66, acquired over 14
593 behavioral sessions.
594
595 Local field potentials were filtered to obtain hippocampal ripples (Blackman filter; 100-
596 300 Hz) and theta oscillations (4-12 Hz)[14]. Hippocampal action potentials that exceeded
597 threshold (60 μV) were aggregated as multiunit activity to measure SPW-R-associated
598 bursts in hippocampal activity. Bursts with peak firing rate exceeding 4 standard
599 deviations above the mean, behaviorally constrained to periods of speed < 10 cm/s, were
600 identified as SPW-R multiunit events. The start and end of each event were defined as
601 the times surrounding the event at which the multiunit firing rate fell back to its mean
602 value. Although ripple power was not an explicit constraint for SPW-R multiunit events,
603 92.8% of SPW-R multiunit events had ripple power exceeding 2 Z scores above baseline
604 (89.0% in replay; 93.5% in nonreplay). The majority of SPW-R events occurred at the
605 force reward sites, where the animals paused longest.
606
607 VTA single-unit activity during single trials was summed over repeated trials in a session
608 to generate peri-event time histograms (PETHs) triggered on the start of SPW-R events.
609 The PETH was smoothed with a Gaussian window (σ=50 ms; similar results were found
610 over a range of σ (30–200 ms). SPW-R modulation amplitude was measured relative to a

300 ms baseline that ended 100 ms before the event, as the baseline-normalized difference between the PETH amplitude measured at the midpoint of the SPW-R event and the mean baseline amplitude. Results were similar using a 5 second baseline ending 1 second before the event. Units with low baseline firing rate (<0.3 Hz) were excluded from analysis to exclude undersampled PETHs. To compute significance of modulation, the SPW-R-aligned raster of each unit was bootstrapped to derive and compare confidence intervals, at the $p<0.05$ level, of a 50 ms bin at the midpoint of the SPW-R event and the average of the confidence intervals of the 300 ms baseline.

Position reconstruction

The animal's location was expressed as a linear distance along the track. For the end-to-end T-maze, the track was linearized by adjoining the 5 segments (**Figure 3- figure supplement 1A,B**). To deal appropriately with the discrete jumps in the linearized representation, a distance look-up table was constructed for all pairs of densely sampled points along the track. We applied a Bayesian estimation algorithm[21,41] to reconstruct position from hippocampal population activity. We expressed the relationship between neuronal activity and position in an encoding model that incorporated spike waveform amplitude features of unsorted spikes in run epochs with speed > 10 cm/s ("clusterless decoding"; only putative pyramidal neuron spikes with peak amplitude > 100 μV and spike width > 300 μs were included). For direction reconstruction, we generated an independent encoding model that related running direction in run epochs to spike waveform amplitude features of unsorted spikes. Using the run velocity threshold of 10 cm/s, reward site arrival and departure were well represented. A non-informative

uniform prior was used as we did not want to impose any spatial-temporal structure on the estimated positions in SPW-R events.

To verify that position on the track could be accurately estimated from hippocampal population activity, we used a cross-validation procedure by dividing run epochs into alternating 1 second training and testing epochs. The rat's position (in 10 cm spatial bins) was estimated in non-overlapping 500 ms time bins in the testing epochs and compared to the true location. Decoding performance was assessed by computing the median error and confusion matrices (**Figure 3- figure supplement 1C)**.

We compared the clusterless decoding paradigm to the standard decoding of spike-sorted units. Spatial tuning curves were constructed for all manually sorted hippocampal place cells with peak place field firing rate > 3 Hz. Median error in clusterless position reconstruction was significantly lower than with spike sorting-based reconstruction (clusterless: 8.3±0.5 cm, spike sorting-based 15.2±1.9 cm, $p<1.22\times10^{-4}$, signed-rank test, n=14). Mean error in clusterless direction reconstruction was 0.26±0.02.

Replay-detection

Replay-detection was performed as described previously[21]. We applied the clusterless Bayesian estimator to non-overlapping, 25 ms bins during SPW-R events occurring in non-run periods (run speed < 10cm/s; **Figure 3- figure supplement 1D)**. Excluding running direction, four paths exist on the SWM task that connect the forced choice reward sites to the free choice reward sites (two of which are correct and two incorrect).

For each SPW-R event, a constant speed trajectory was fitted to the sequence of position estimates[21,22] for each of the four possible paths. The best fitting trajectory was selected based on a goodness-of-fit score ("replay score"), computed as the mean posterior probability within 15 cm of the fitted trajectory. To test if fitted trajectories could be expected by chance alignment of position estimates, the replay score for each candidate event was compared to replay score distributions derived with two shuffles of the data, using the approach described in reference 21. The first "column cycle shuffle" controls for the linear alignment of consecutive position estimates by circularly shifting the estimated probability distribution over position (PDF) in each candidate event time bin by a random distance. The second "pseudo-event shuffle" controls for bias towards particular locations, by constructing artificial candidate events generated by replacing each PDF in a candidate event with a PDF drawn at random from the complete set of candidate events in each session. Each shuffle was performed 1500 times for each candidate event to obtain sample distributions of the replay score. To increase detection sensitivity of possible replay events on the spatial working memory task, we considered replay events to be those with a Monte Carlo p value < 0.05 for both shuffles on at least one path. We considered non-replay enriched events those with a p value > 0.2 for both shuffles for all four trajectories. For replay content assessments (below), we used a more stringent criterion for replay detection by performing the shuffles for each putative replay event on the one trajectory with the strongest replay score. We obtained similar results using the standard criterion.

Replay/total (R/T) SPW-R events for each session (s) are as follows: R/T rat 1, s1 173/798; s2 141/434; s3 92/425; s4 71/344; s5 55/203; rat2, s1 120/377; s2 48/210; s3 68/219; rat 3, s1 78/241; s2 30/93; rat 4, s1 65/328; s2 53/275; s3 49/234; s4 64/464; rat 5, s1 -/627; rat 5, s2 -/904.

Replay content assessment

Distributions of replayed spatial locations were derived by accumulating the spatial posterior probability distribution function across all 25 ms time bins of all replay events, in each recording, for SPW-Rs that occurred while the rat paused at forced reward locations. We determined the temporal delay between hippocampal SPW-R events and VTA activity on the basis of the delay in the SPW-R event-triggered VTA local field potential (84±13 ms). The distribution of VTA spike-associated replay content was derived by accumulating the spatial probability distribution functions for the subset of 25 ms replay time bins that preceded VTA unit spikes by this fixed delay. The probability of reward site content for each recording was measured as the fraction of the distribution of replayed spatial locations that was associated with reward sites. The probability of VTA units coordinating with reward site content (reward site probability) was measured similarly, as the fraction of the distribution of VTA spike-associated replay content that was associated with reward locations. To compare RR and nonRR VTA spike-associated replay content with overall replay content, we computed a reward site bias as follows: Each replay time bin was assigned a 1 (or 0) when the average representation of reward site regions exceeded (or did not exceed) the average representation of nonreward regions. The same binary metric was applied to each RR and nonRR VTA spike-

703 associated replay time bin. From these measures, we computed across the entire dataset
704 the proportion of VTA spike-associated replay time bins that better represented reward
705 site regions compared to nonreward site regions, and we compared this with the
706 proportion of replay time bins that better represented reward site regions, accounting for
707 differences in the number of spike-associated time bins across RR units and nonRR units
708 across recordings, to derive the excess reward site bias. There were 5422 replay time
709 bins, 2269 RR unit spike-associated bins, and 2455 nonRR unit spike-associated bins.
710 On the SWM task, there were 3554 replay time bins and 1046 RR unit spike-associated
711 bins. On the linear track, there were 1868 replay time bins and 818 RR unit spike-
712 associated bins. The reward site bias was highly correlated with the reward site
713 probability (RR units, $r=0.80$, $p=1.36\times10^{-4}$). To explore the sensitivity of the reward site
714 bias to the temporal delay between replayed spatial content and VTA unit activity, we
715 systematically varied the delay in 25 ms steps. Consistent with the latency of the SPW-
716 R-associated VTA potential, the excess reward site bias of RR units was maximal at a 75
717 ms VTA lag relative to hippocampal activity (data not shown).
718
719 To evaluate whether RR unit coordination with replayed reward site representations
720 correlated with choice behavior, we measured the excess reward site bias at force reward
721 site locations immediately after correct and error trials; and separately, immediately prior
722 to correct and error trials. There were 616 RR unit spike-associated bins following
723 correct trials, 243 following error trials, 565 prior to correct trials, and 142 prior to error
724 trials.
725

For forward and reverse replay content analyses, we measured the reward site bias of replay event time bins that showed strong directional preference for outbound (O) or inbound (I) track direction (|direction index|>0.5, where the direction index is (O-I)/(O+I))[42]. For each replay event, we transformed the direction index of each time bin into an index of forward or reverse content, as follows. Since we restricted our analysis to replay events occurring while the rat paused at force reward sites, for centrifugal sequence replay away from the animal's location, outbound content reflects forward replay, while inbound content reflects reverse replay. In contrast, for remotely initiated, centripetal replay towards the animal's location, inbound content reflects forward replay, while outbound content reflects reverse replay. For centrifugal and centripetal replay content analyses, we aggregated forward and reverse replay event time bins together, defining centrifugal replay events as replay trajectories moving away from the current position of the animal and centripetal replay events as replay trajectories approaching the animal. We compared the reward site bias of centrifugal and centripetal replay event time bins and of forward and reverse replay event time bins to the reward site bias of VTA unit spikes occurring with 84 ms delay to those replay time bins. There were 1700 time bins with centrifugal replay content, of which 681 were associated with RR unit spikes and 770 with nonRR unit spikes. There were 1248 time bins with centripetal replay content, of which 585 were associated with RR unit spikes and 602 with nonRR unit spikes. In addition, there were 1561 time bins with forward replay content, of which 699 were associated with RR unit spikes and 720 with nonRR unit spikes. There were 1313 time bins with reverse replay content, of which 567 were associated with RR unit spikes and 652 with nonRR unit spikes.

There were several cases in which we sought to determine whether the excess reward site bias of VTA units compared to hippocampal replay was greater across two comparisons (B vs A compared to C vs A): 1) excess reward site bias of RR units versus nonRR units; 2) excess reward site bias of RR units on the SWM task versus on the linear track; 3) excess reward site bias of RR units after correct trials versus after error trials; 4) excess reward site bias of RR units before correct trials versus before error trials; and 5) excess reward site bias of RR units at forward and reverse replay. For each case, we ran a logistic regression in which we considered each element of the case separately, as well as their interaction. For example, in the first case, we computed a logistic regression to measure the interaction between RR unit-associated reward site bias and replay-associated reward site bias, and nonRR unit-associated reward site bias and replay associated reward site bias. We then compared the interaction term to a distribution of simulated interaction terms assuming the null hypothesis. We considered the reward site bias for replay (A), the reward site bias for RR units (B), and the reward site bias for nonRR units (C). The logistic regression predicted reward site bias as a binary dependent variable (present/absent) with binary predictors of (either B or C = 1 vs A = 0), comparison (B vs A = 1, C vs A = 0), and their interaction, the latter being the predictor pertinent to the research question. Since these hypotheses were in only one direction, we ran 1-tail tests. In order to determine the one tail *p* value in these nonlinear tests, we performed a nonparametric permutation test of 1,000 iterations of the logistic regression, assuming the null hypothesis (i.e., the coefficient for the interaction is centered at zero). In each iteration, the fraction of reward site bias (A) for each comparison was taken as

772 the overall average of actual estimates separately incremented with a perturbation from a
773 normal distribution. The mean of this distribution was set to 0 and the standard deviation
774 chosen so as to produce simulated interaction regression coefficients with a standard
775 deviation approximately equal to the standard error for the same predictor estimated from
776 the logistic regression of the actual data. The proportion of simulated interaction
777 coefficients greater than or equal to the actual interaction coefficient was taken as the
778 estimated one-tail *p* value.
779
780 To test for bias in the reconstruction algorithm towards reward sites, we first decoded the
781 estimated position of nonreplay events. We did not detect a bias for reward sites in the
782 distribution of spatial locations across nonreplay events (reward site bias 0.424±0.004;
783 probability/spatial bin of content at reward locations 0.032±0.007 bin^{-1}; non-reward
784 locations 0.023±0.003 bin^{-1}; p=0.1, signed-rank test, n=14 recordings). Because SPW-R
785 events may encode hippocampal spatial representations other than replay sequences, and
786 because we may have miscategorized some replay events as nonreplay events, we also
787 assessed the output of the reconstruction algorithm in the absence of hippocampal
788 activity. This approach did not detect a preference in the decoder toward reward sites
789 (probability/spatial bin of content at reward locations 0.029±0.006 bin^{-1}; non-reward
790 locations 0.023±0.003 bin^{-1}; p=0.6, signed-rank test, n=14 recordings).
791
792 **Theta phase analysis**
793 The Hilbert transform of the theta-filtered LFP was used to assess theta phase
794 relationships of VTA units. To evaluate for theta phase preference of VTA units, we

795 computed Rayleigh's test for uniformity of the circular theta phase distribution of each
796 VTA neuron's spikes against a unimodal alternative; and we computed the parameters
797 mu and kappa of the von Mises distribution that best fit that distribution[14,23], using
798 custom Matlab code. The circular concentration coefficient kappa is inversely related to
799 the variance of the distribution, such that in the limit of kappa = 0, the circular
800 distribution is uniform.
801
802 **Frame analysis**
803 Frames were identified as described previously[27], within epochs of SWS defined on the
804 basis of low hippocampal theta/delta ratio and clear sleep posture (SWS median duration,
805 range: 1226 seconds, 793-1998 seconds). Within SWS epochs, multiunit activity from all
806 tetrodes were combined, counted in 10 ms bins, and smoothed with a Gaussian window,
807 with σ=30 ms. Frames were identified as periods of high activity between silent periods,
808 with the spike count threshold defined as the spike count at which the spike count
809 distribution reached its first minimum (in 10 ms bins). Clusterless reconstruction was
810 applied to frames of SWS to derive the spatial probability distribution function of each 25
811 ms time bin within each frame. Spatial content per frame was taken as the average of the
812 maximum decoded probability of each time bin.
813
814 **Acknowledgements**
815 We thank J. Locascio for statistical support for the logistic regression permutation
816 analysis. We thank H. Penagos, G. Hale, and K. Neville for comments on the
817 manuscript. This work was supported by an NIH grant to M.A.W. (R01-MH061976), an

ONR-MURI grant to M.A.W. (N00014-10-1-0936), and a mentored NIH grant to S.N.G. (K08-MH-81207-01A1).

Competing interests statement:

The authors declared no competing interests.

References

1. O'Keefe, J. & Dostrovsky, J.. The hippocampus as a spatial map. Preliminary evidence from unit activity in the freely-moving rat. *Brain Res.* **34**, 171–175 (1971).

2. Lee, A.K. & Wilson, M.A. Memory of sequential experience in the hippocampus during slow wave sleep. *Neuron*. **36**, 1183-1194 (2002).

3. Foster, D.J. & Wilson, M.A. Reverse replay of behavioural sequences in hippocampal place cells during the awake state. *Nature*. **440**, 680-683 (2006).

4. Diba, K. & Buzsáki, G. Forward & reverse hippocampal place-cell sequences during ripples. *Nat Neurosci*. **10**, 1241-1242 (2007).

5. Jadhav S.P., Kemere, C., German, P.W. & Frank, L.M. Awake hippocampal sharp-wave ripples support spatial memory. *Science*. **336**:1454-1458 (2012). doi: 10.1126/science.1217230

6. Girardeau, G., Benchenane, K., Wiener, S.I., Buzsáki, G. & Zugaro, M.B. Selective suppression of hippocampal ripples impairs spatial memory. *Nat Neurosci*. **12**, 1222-1223 (2009). doi: 10.1038/nn.2384.

7. Ego-Stengel, V. & Wilson, M.A. Disruption of ripple-associated hippocampal activity during rest impairs spatial learning in the rat. *Hippocampus*. **20**, 1-10 (2010). doi: 10.1002/hipo.20707.

8. Singer, A.C. & Frank, L.M. Rewarded outcomes enhance reactivation of experience in the hippocampus. *Neuron*. **64**, 910-921 (2009). doi: 10.1016/j.neuron.2009.11.016.

9. Karlsson MP, Frank LM. Awake replay of remote experiences in the hippocampus. *Nat Neurosci*. **12**:913-8 (2009). doi: 10.1038/nn.2344.

10. Schultz, W. Predictive reward signal of dopamine neurons. *J Neurophysiol*. **80**, 1-27 (1998).

11. Montague, P.R., Dayan, P. & Sejnowski, T.J. A framework for mesencephalic dopamine systems based on predictive Hebbian learning. *J Neurosci*. **16**, 1936-1947 (1996).

12. McNamara CG, Tejero-Cantero Á, Trouche S, Campo-Urriza N, Dupret D. Dopaminergic neurons promote hippocampal reactivation and spatial memory persistence. *Nat Neurosci*. **17**:1658-60 (2014). doi: 10.1038/nn.3843.

13. de Lavilléon G, Lacroix MM, Rondi-Reig L, Benchenane K. Explicit memory creation during sleep demonstrates a causal role of place cells in navigation. *Nat Neurosci*. **18**:493-495 (2015). doi: 10.1038/nn.3970.

14. Jones, M.W. & Wilson, M.A. Theta rhythms coordinate hippocampal-prefrontal interactions in a spatial memory task. *PLoS Biol*. **3**,e402. (2005). http://www.plosbiology.org/article/info%3Adoi%2F10.1371%2Fjournal.pbio.0030402

15. Morris G, Nevet A, Arkadir D, Vaadia E, Bergman H. Midbrain dopamine neurons encode decisions for future action. *Nat Neurosci*. **9**:1057-63 (2006).

16. Roesch MR, Calu DJ, Schoenbaum G. Dopamine neurons encode the better option in rats deciding between differently delayed or sized rewards. *Nat Neurosci*. **10**:1615-24 (2007).

17. Totah NK, Kim Y, Moghaddam B. Distinct prestimulus and poststimulus activation of VTA neurons correlates with stimulus detection. *J Neurophysiol*. **110**:75-85 (2013). doi: 10.1152/jn.00784.2012.

885 18. Fujisawa, S. & Buzsáki, G. A 4 Hz oscillation adaptively synchronizes prefrontal,
886 VTA, & hippocampal activities. *Neuron*. **72**, 153-165 (2011). doi:
887 10.1016/j.neuron.2011.08.018.
888
889 19. Ungless, M.A. & Grace, A.A. Are you or aren't you? Challenges associated with
890 physiologically identifying dopamine neurons. *Trends Neurosci*. **35**, 422-430 (2012). doi:
891 10.1016/j.tins.2012.02.003.
892
893 20. Kloosterman, F., Layton, S., Chen, Z. & Wilson, M.A. Bayesian decoding using
894 unsorted spikes in the rat hippocampus. *J. Neurophysiol*. **11**,217-227 (2014). doi:
895 10.1152/jn.01046.2012.
896
897 21. Davidson, T.J., Kloosterman, F. & Wilson, M.A. Hippocampal replay of extended
898 experience. *Neuron*. **63**, 497-507 (2009). doi: 10.1016/j.neuron.2009.07.027.
899
900 22. Kloosterman, F. Analysis of Hippocampal Memory Replay Using Neural Population
901 Decoding..*Neuronal Network Analysis*. 259-282. (Springer, New York, 2012).
902
903 23. Siapas AG, Lubenov, EV, Wilson MA. Prefrontal phase locking to hippocampal theta
904 oscillations. *Neuron* **46**: 141-151 (2005).
905

906 24. Pavlides, C. & Winson, J. Influences of hippocampal place cell firing in the awake
907 state on the activity of these cells during subsequent sleep episodes. *J Neurosci*. **9**, 2907-
908 2918 (1989).
909
910 25. Wilson, M.A. & McNaughton, B.L. Reactivation of hippocampal ensemble memories
911 during sleep. *Science*. **265**, 676-679 (1994).
912
913 26. Nádasdy, Z., Hirase, H., Czurkó, A., Csicsvari, J. & Buzsáki, G. Replay & time
914 compression of recurring spike sequences in the hippocampus. *J Neurosci*. **19**, 9497-9507
915 (1999).
916
917 27. Ji, D. & Wilson, M.A. Coordinated memory replay in the visual cortex &
918 hippocampus during sleep. *Nat Neurosci*. **10**, 100 - 107 (2007).
919
920 28. Pennartz CM, Lee E, Verheul J, Lipa P, Barnes CA, McNaughton BL. The ventral
921 striatum in off-line processing: ensemble reactivation during sleep and modulation by
922 hippocampal ripples. *J Neurosci*.;**24**:6446-56 (2004).
923
924 29. Lansink CS, Goltstein PM, Lankelma JV, McNaughton BL, Pennartz CM.
925 Hippocampus leads ventral striatum in replay of place-reward information. *PLoS Biol*.
926 2009;**7**:e1000173. doi: 10.1371/journal.pbio.1000173. Epub 2009 Aug 18.
927

928 30. Schultz W, Apicella P, Scarnati E, Ljungberg T. Neuronal activity in monkey ventral
929 striatum related to the expectation of reward. *J Neurosci*.;**12**:4595-610 (1992).
930
931 31. Cardinal RN, Parkinson JA, Hall J, Everitt BJ. Emotion and motivation: the role of
932 the amygdala, ventral striatum, and prefrontal cortex. *Neurosci Biobehav Rev*.;**26**:321-52
933 (2002).
934
935 32. Cohen, J.Y., Haesler, S., Vong, L., Lowell, B.B. & Uchida, N. Neuron-type-specific
936 signals for reward & punishment in the ventral tegmental area. *Nature*. **482**, 85-88
937 (2012). doi: 10.1038/nature10754.
938
939 33. Lammel S, Hetzel A, Häckel O, Jones I, Liss B, Roeper J. Unique properties of
940 mesoprefrontal neurons within a dual mesocorticolimbic dopamine system. *Neuron.*
941 **57**:760-773 (2008). doi: 10.1016/j.neuron.2008.01.022.
942
943 34. Margolis EB, Toy B, Himmels P, Morales M, Fields HL. Identification of rat ventral
944 tegmental area GABAergic neurons. *PLoS One* **7**:e42365 (2012). doi:
945 10.1371/journal.pone.0042365. Epub 2012 Jul 31.
946
947 35. Hnasko TS, Hjelmstad GO, Fields HL, Edwards RH. Ventral tegmental area
948 glutamate neurons: electrophysiological properties and projections. *J Neurosci*.
949 **32**:15076-85 (2012). doi: 10.1523/JNEUROSCI.3128-12.2012.
950

951 36. Margolis EB, Lock H, Hjelmstad GO, Fields HL. The ventral tegmental area
952 revisited: is there an electrophysiological marker for dopaminergic neurons? *J Physiol.*
953 **577**, 907-24 (2006).
954
955 37. Walsh, M.M. & Anderson, J.R.. Navigating Complex Decision Spaces: Problems and
956 Paradigms in Sequential Choice. *Psychol Bull*. **140**, 466-86. (2014). doi:
957 10.1037/a0033455
958
959 38. Doll, B.B., Simon, D.A. & Daw, N.D. The ubiquity of model-based reinforcement
960 learning. *Curr Opin Neurobiol*. **22**, 1075-1081 (2012). doi: 10.1016/j.conb.2012.08.003.
961
962 39. Pfeiffer, B.E. & Foster, D.J. Hippocampal place-cell sequences depict future paths to
963 remembered goals. *Nature*. **497**, 74-79 (2013). doi: 10.1038/nature12112
964
965 40. Paxinos, G. & Watson, C. *The rat brain in stereotaxic coordinates*. (Academic Press,
966 London, 1998).
967
968 41. Zhang K, Ginzburg I, McNaughton BL, Sejnowski TJ. Interpreting neuronal
969 population activity by reconstruction: unified framework with application to hippocampal
970 place cells. *J Neurophysiol*. **79**,1017-1044 (1998).
971

42. Singer AC, Carr MF, Karlsson MP, Frank LM. Hippocampal SWR activity predicts correct decisions during the initial learning of an alternation task. *Neuron*.**77**:1163-73 (2013). doi: 10.1016/j.neuron.2013.01.027

Author contributions

S.N.G. and M.A.W. designed the experiment, S.N.G. performed the experiment and analyzed the data, F.K. developed the clusterless reconstruction algorithm, and S.N.G. and M.A.W. wrote the paper.

Author information

Correspondence and requests for materials should be addressed to gomperts.stephen@mgh.harvard.edu.

Figure 1. Spatial working memory task and VTA unit properties. A, Spatial working memory task. In the force direction (sample phase), rats traverse the central arm for reward (R) at either of two pseudorandomly selected left or right force-reward locations. The reward contingency in the choice direction (test phase) required that if the rat had been forced to turn left (or right) in the sample phase, then the correct response in the test phase was to turn right (or left, respectively). **B,** Example VTA unit's average reward site responses for correct trials (solid line) and error trials (dashed line). The nosepoke occurs at 0 seconds. The profile of reward-site associated activity, including differential activity on correct versus error trials during reward approach and during reward acquisition, is consistent with prior observations in instrumental tasks[15,16,17]. **C,** Waveform features of 145 VTA units recorded in the sleep box, using the waveform criteria described in [18]. The waveform duration is defined as the time from waveform major peak to final peak. The trough to peak ratio is defined as the ratio of the waveform trough amplitude to the full amplitude. 84 units that were acquired with adequate task behavior and co-recorded hippocampal activity underwent further analysis. Reward responsive (RR) units are shown in blue, and non-reward responsive units (nonRR) are shown in red. Waveforms of two units are displayed.

Figure 2. VTA unit coordination with hippocampal sharp-wave ripples.

A, Continuous recordings of hippocampal (HC) (**1**) single unit activity**,** (**2**) multiunit activity (MUA, average spike rate per tetrode), (**3**) local field potential and ripple band, (**4**) a simultaneously recorded reward-responsive (RR) VTA unit, and (**5**) the animal's position on the track. The hippocampal units are ordered by the position of their place fields on the spatial working memory task. Sharp-wave ripple events (SPW-R) are shown in gray. **B,** A magnified view of 10 seconds of continuous data. **C1,** Rastered RR VTA unit action potentials, (**2)** RR VTA unit peri-event time histogram (PETH; smoothing with a 50ms Gaussian window), and (**3)** HC multiunit PETH (10 ms Gaussian smoothing), aligned to the start of SPW-R-associated HC multiunit events.

Figure 2- figure supplement 1. **Firing rate distributions of SPW-R modulated VTA units at reward acquisition and at SPW-R events of quiet wakefulness.** For units recorded on the SWM task, the average nosepoke triggered PETH for correct trials (solid blue lines) and for error trials (red dashed lines) are shown. Units acquired on the linear maze have a single nosepoke triggered PETH. Data are aligned to the time of nosepoke (vertical line). For the SPW-R event triggered PETH plots, data are aligned to the start of SPW-R events. Note that VTA unit activity often increases during reward approach and reward acquisition, and that VTA unit activity can be both positively and negatively modulated at SPW-R events.

Figure 3. Modulation depth of VTA reward responsive units at hippocampal SPW-R events depends on SPW-R spatial content. A, Rastered reward responsive (RR) unit spikes (**1**) and RR unit and hippocampal (HC) multiunit PETHs (**2,3**), aligned to the start of SPW-R events encoding replay sequences. **B,** As in **A**, for SPW-R events not encoding replay. **C,** PETH modulation depth of RR units (blue) is greater for replay than nonreplay events; $p=4.5\times10^{-4}$, signed-rank test). NonRR unit data are shown in red ($p=0.6$). Solid circles with error bars designate the mean and s.e.m. for RR and nonRR units.

Figure 3- figure supplement 1. Position reconstruction using clusterless hippocampal decoding. **A,** Bayesian reconstruction of run behavior on the spatial working memory task (500 ms time bins). The track has been linearized. **B,** Decomposition of the track into segments for linearization. Maze segments were apposed in the direction of run in the choice direction: from force reward sites (R3, R4) to force point (fp) to choice point (cp) to choice reward sites (R1, R2). **C,** Confusion plot for this recording session, using alternating 1 second epochs for training and testing the reconstruction algorithm. **D1,** Bayesian reconstruction of a SPW-R event reveals spatial sequence reactivation (25 ms time bins). **D2,** The associated hippocampal multiunit activity. **D3,** The action potentials of two simultaneously recorded reward responsive VTA units.

Figure 3- figure supplement 2. Ripple power, SPW-R associated hippocampal activity, and SPW-R event latency in the immediate post-reward period were similar for replay and non-replay events. A1, For the recording shown in **Figure 3AB**, cumulative ripple-band power of replay (green solid line) and non-replay (brown dashed line) events are displayed. **A2,** Across recordings, replay and nonreplay events have similar ripple power (box and whisker plots, medians with interquartile range; p=1, sign-rank test). **B1,** Cumulative SPW-R event peak multiunit activity (MUA; Hz/tetrode) for the same example, for replay (green solid) and non-replay (brown dashed) events. **B2,** Across recordings, SPW-R event peak MUA is similar for replay and non-replay events (medians with interquartile range; p=0.6, sign-rank test). **C.** Cumulative distributions of SPW-R event latencies relative to nosepoke for reward delivery were similar for replay and nonreplay SPW-R events (p=0.2, Kolmogorov-Smirnov test).

Figure 4. Reward responsive VTA units coordinate with replayed reward locations. **A,** The SPW-R triggered VTA local field potential (LFP) shows a delayed potential. Time 0 reflects the start of SPW-R events. **B,** Incorporating this delay between the hippocampus and VTA, across replay events occurring at the forced reward sites, RR unit spikes preferentially coordinated with replayed reward locations compared to SPW-R replay content in general (p=0.048, chi=3.9, Chi-square test) and compared to nonRR units (p=0.016, nonparametric permutation test). Error bars represent s.d. **C,** Probability distribution of replayed spatial locations for replay events occurring at the forced reward sites on the spatial working memory (SWM) (**1**) and linear tasks (**2**) (10 cm bins), accumulated across recordings. Dashed boxes designate reward sites. **D,E,** Distribution of replayed locations coinciding with RR unit spikes (**D1,2**) and nonRR unit spikes (**E1,2**), adjusting for the latency between SPW-R onset and the VTA delayed potential. The probability colorbar for the SWM task ranges from 0 to 0.04 and for the linear track ranges from 0 to 0.1.

Figure 5. The bias of reward responsive VTA unit activity towards the replay of reward locations is greater for centrifugal than centripetal replay. A1,2, Bayesian reconstruction of run position and run direction on the linear track (500 ms time bins). Outbound refers to run direction from 0 to 200 cm. **A3,** Position confusion plot for this recording session, using alternating 1 second epochs for training and testing the reconstruction algorithm. **A4,** Run direction confusion plot. **B,** Centrifugal, forward replay event occurring while the rat paused at the far reward site (190 cm; black circle indicates the rat's position). **B1,** Position reconstruction (25 ms time bins). **B2,** direction reconstruction). **B3**, The associated hippocampal multiunit activity. **C,** Centripetal, forward replay event occurring while the rat paused at the far reward site. **C1**, Position reconstruction. **C2**, Direction reconstruction. **C3**, Associated hippocampal multiunit activity. **D,** Across centrifugal replay time bins, RR unit spikes preferentially coordinated with replay of reward locations compared to centrifugal replay content in general (p=0.014, chi=6.0, Chi-square test) and compared to nonRR units at centrifugal replay (p=0.05, nonparametric permutation test). Error bars represent s.d. **E,** Across centripetal replay time bins, RR unit spikes showed no increase in coordination with replay of reward locations compared to centripetal replay content in general (p=0.5, chi=0.5, Chi-square test). Error bars represent s.d.

Figure 5- figure supplement 1. Centrifugal and centripetal replayed locations associated with RR unit activity on the SWM task and the linear track.

A, On the SWM task, the distribution of centrifugal replayed locations (green) is less concentrated at reward sites (marked by vertical lines) than the distribution of RR unit-associated centrifugal replayed locations (blue). See Figure 5 for statistics. Maze segments were aggregated by apposing them in the direction of run in the choice direction: from force reward sites (R3, R4) to force point (fp) to choice point (cp) to choice reward sites (R1, R2). Spatial bins 1-10 show the average of the force arms of the task (arms 3 and 4), spatial bins 11-20 show the central arm, and spatial bins 21-30 show the average of the choice arms (arms 1 and 2). **B,** The distribution of centripetal replayed locations (green) on the SWM task is similar to the distribution of RR unit-associated centripetal replayed locations (blue). **C**, On the linear track, the distributions of centrifugal replayed locations (green) and RR unit-associated centrifugal replayed locations (blue) are similar. **D**, On the linear track, the distribution of centripetal replayed locations (green) and the distribution of RR unit-associated centripetal replayed locations (blue) are also similar.

Figure 6. VTA units coordinate with hippocampal theta. A, Spike times of a reward responsive (RR) VTA unit relative to hippocampal theta and raw LFP during running behavior, and spike phase distribution (circular concentration coefficient, kappa = 0.14; Rayleigh statistic *p* value = 0.002). **B,** Circular concentration at hippocampal theta is greater for RR units than nonRR units (p=0.031, rank-sum test). Error bars represent s.e.m. **C,** The probability of replayed reward locations coinciding with the spikes of theta-modulated RR units correlates with the circular concentration of those units at hippocampal theta (r=0.51, p=0.038).

Figure 7. SPW-R-associated modulation of VTA units during periods of quiet wakefulness (QW) on the task and during subsequent slow wave sleep (SWS). A, Rastered QW-associated reward responsive (RR) VTA unit spikes (**1**) and RR unit and hippocampal (HC) multiunit PETHs (**2,3**), aligned to SPW-R events. **B,** SWS-associated data for the same RR unit. **C,** SPW-R event modulation depth of RR and nonRR unit activity in QW and SWS (RR units: QW vs SWS, p=0.003, rank-sum test; nonRR units: QW vs SWS, p=0.13, rank-sum test). Error bars represent s.e.m. **D1,** Hippocampal multiunit activity, (**2**) ripple band, and (**3**) two RR VTA units in SWS. **E,** Distributions of (**1**) SWS frame duration and (**2)** interframe duration across recordings. **F,** Cumulative distribution of within-frame SPW-R frequency. **G**, Within-frame VTA unit activity. RR units are shown separately in dashed line. **H,** The difference in each VTA unit's activity at frames of high and low SPW-R rate, defined relative to the mean (RR units: p=0.003, signed-rank test; nonRR units: p=0.5). **I,** The difference in mean spatial content of frames with high and low VTA unit activity, relative to the mean (RR units: p=0.045, signed-rank test).

Figure 8. Histological location of tetrode tips targeting the VTA. For each rat, electrolytic lesions marked the tetrode tip locations, and these were mapped onto the stereotaxic atlas of Paxinos and Watson (1998). Tetrode tips under-represent recording locations, which were acquired as electrodes were systematically lowered within the VTA along their tracks. SNR, substantia nigra reticulata.

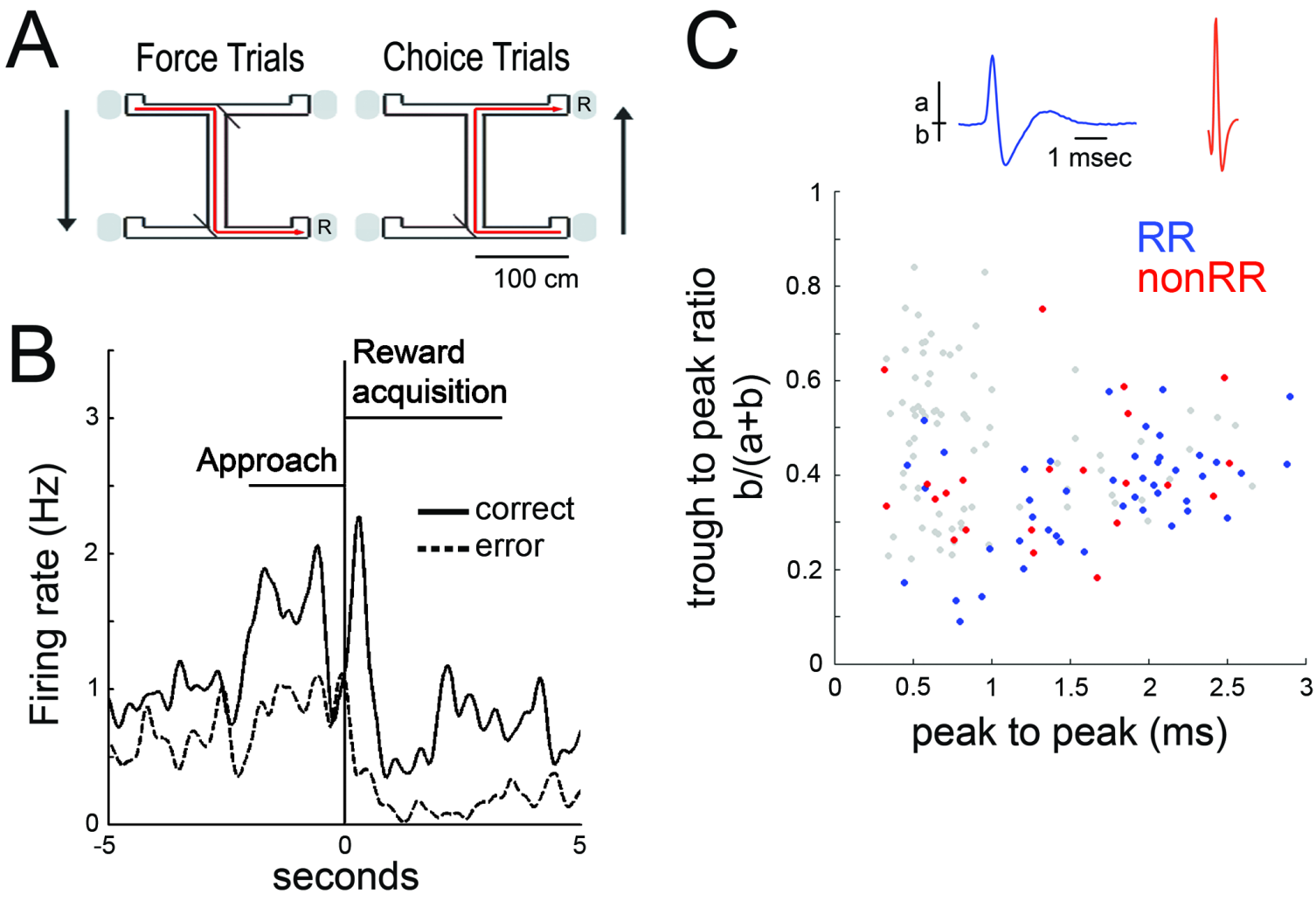
A
Force Trials
Choice Trials
R
R
100 cm
B
Reward
acquisition
Approach
correct
error
Firing rate (Hz)
seconds
C
a
b
1 msec
RR
nonRR
trough to peak ratio
b/(a+b)
peak to peak (ms)

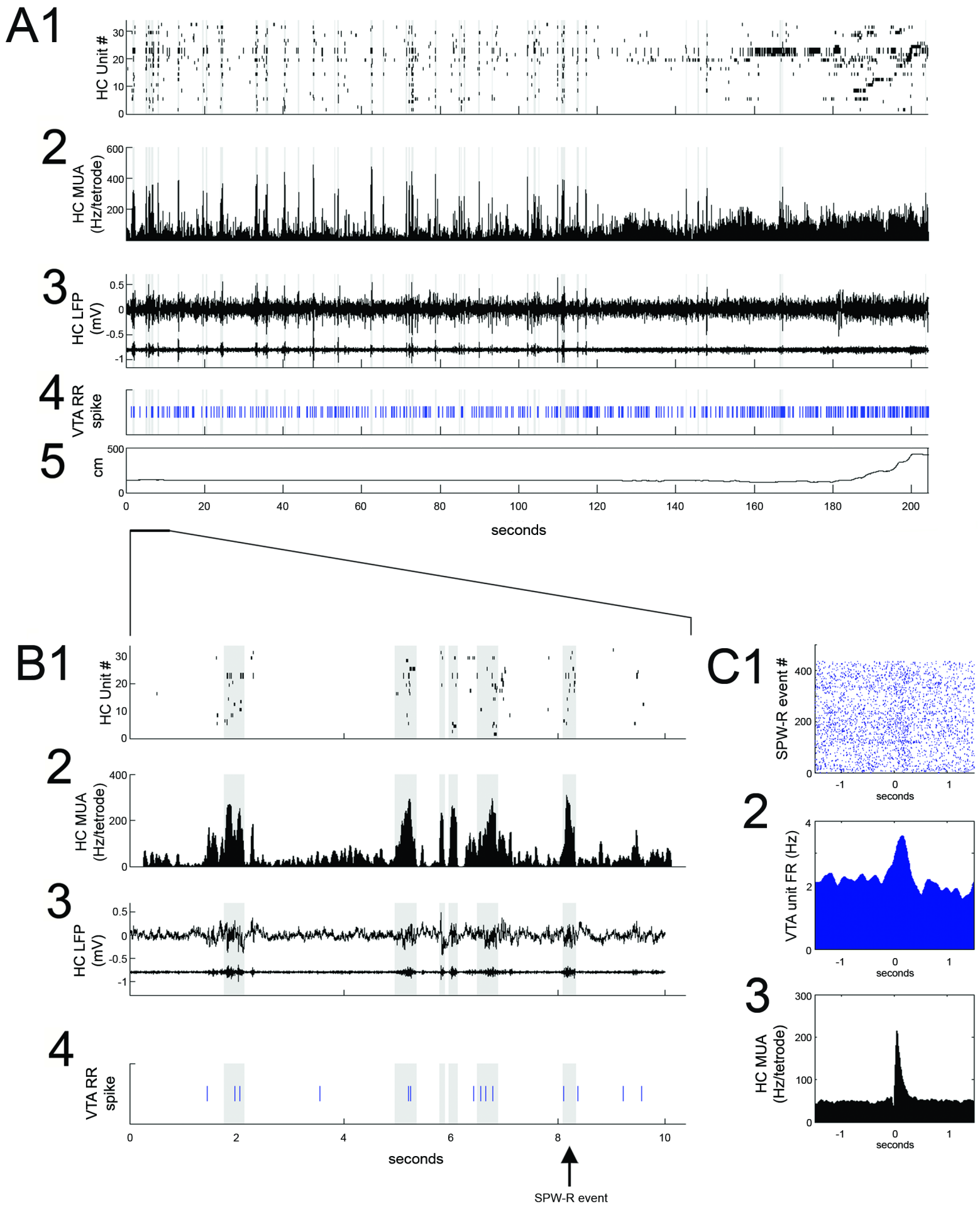
A1
HC Unit #
2
HC MUA (Hz/tetrode)
3
HC LFP (mV)
4
VTA RR spike
5
cm
seconds
B1
HC Unit #
2
HC MUA (Hz/tetrode)
3
HC LFP (mV)
4
VTA RR spike
seconds
SPW-R event
C1
SPW-R event #
seconds
2
VTA unit FR (Hz)
seconds
3
HC MUA (Hz/tetrode)
seconds

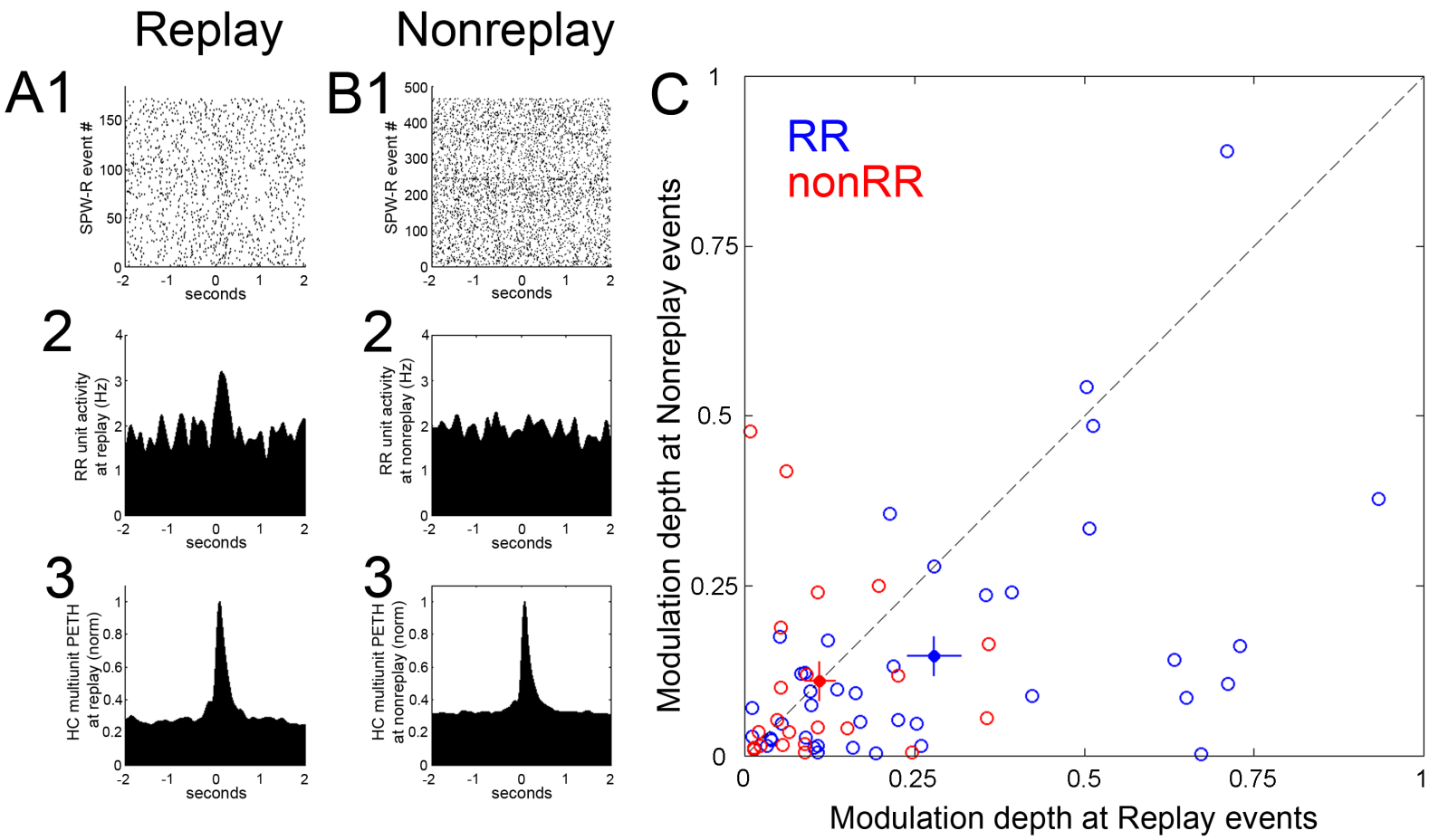
Replay
Nonreplay
A1
B1
C
SPW-R event #
seconds
2
RR unit activity at replay (Hz)
RR unit activity at nonreplay (Hz)
3
HC multiunit PETH at replay (norm)
HC multiunit PETH at nonreplay (norm)
RR
nonRR
Modulation depth at Nonreplay events
Modulation depth at Replay events

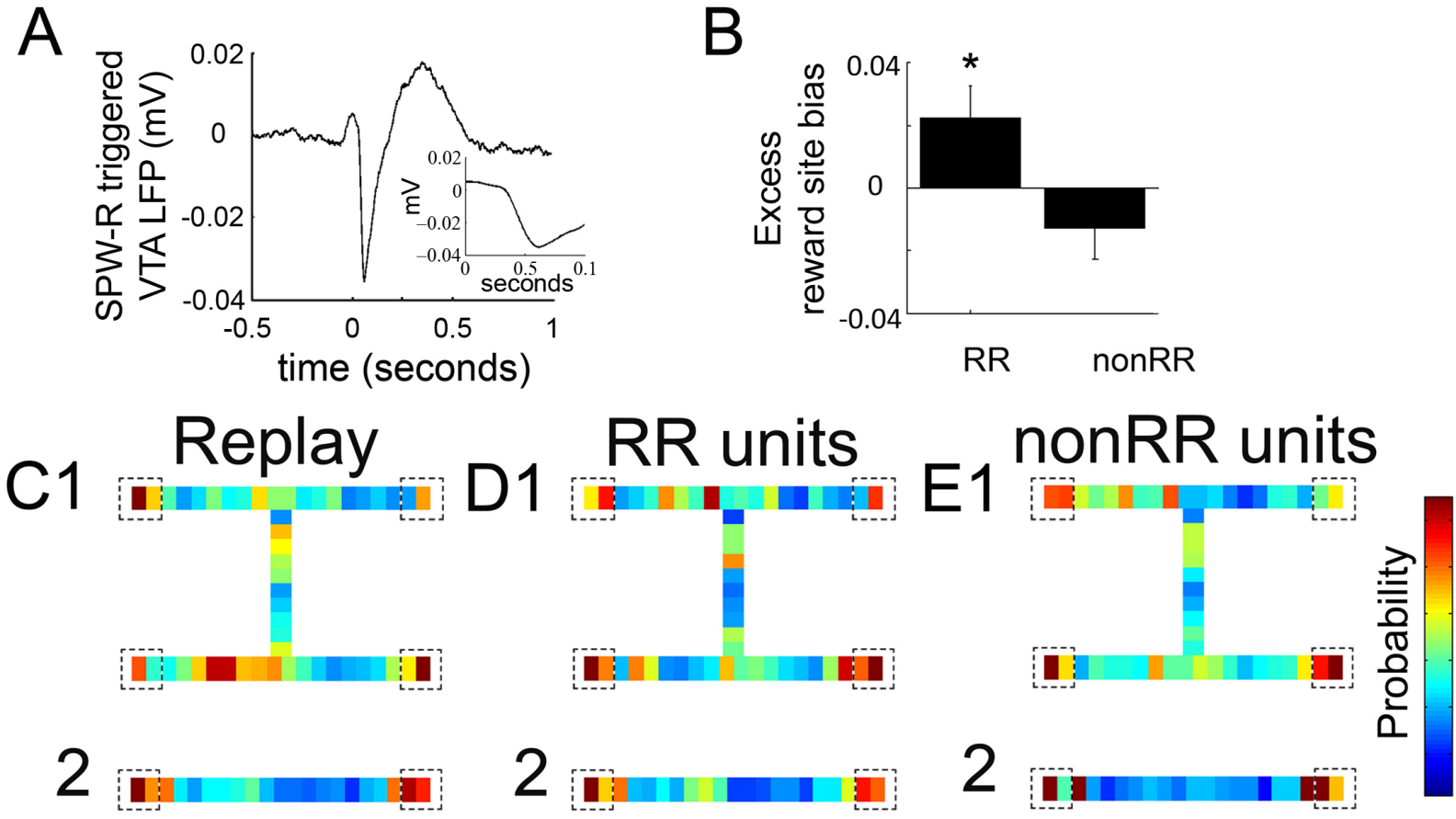
A
SPW-R triggered
VTA LFP (mV)
0.02
0
-0.02
-0.04
-0.5
0
0.5
1
time (seconds)
mV
0.02
0
−0.02
−0.04
0
0.5
0.1
seconds
B
Excess
reward site bias
0.04
0
-0.04
*
RR
nonRR
C1
Replay
2
D1
RR units
2
E1
nonRR units
2
Probability

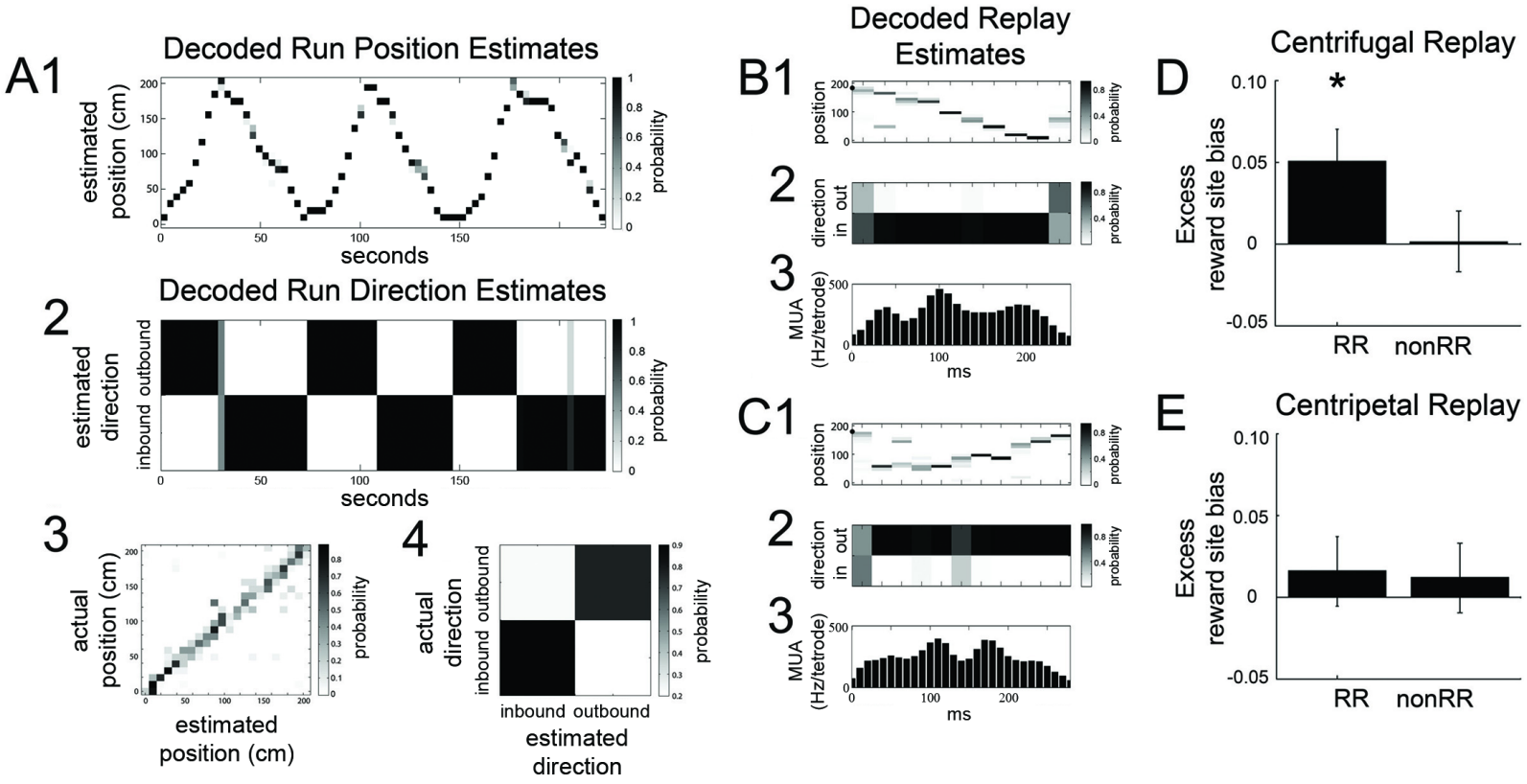
A1
Decoded Run Position Estimates
estimated position (cm)
seconds
probability
2
Decoded Run Direction Estimates
estimated direction
inbound outbound
seconds
probability
3
actual position (cm)
estimated position (cm)
probability
4
actual direction
inbound outbound
estimated direction
probability
Decoded Replay Estimates
B1
position
probability
2
direction
in out
probability
3
MUA (Hz/tetrode)
ms
C1
position
probability
2
direction
in out
probability
3
MUA (Hz/tetrode)
ms
D
Centrifugal Replay
Excess reward site bias
RR
nonRR
E
Centripetal Replay
Excess reward site bias
RR
nonRR

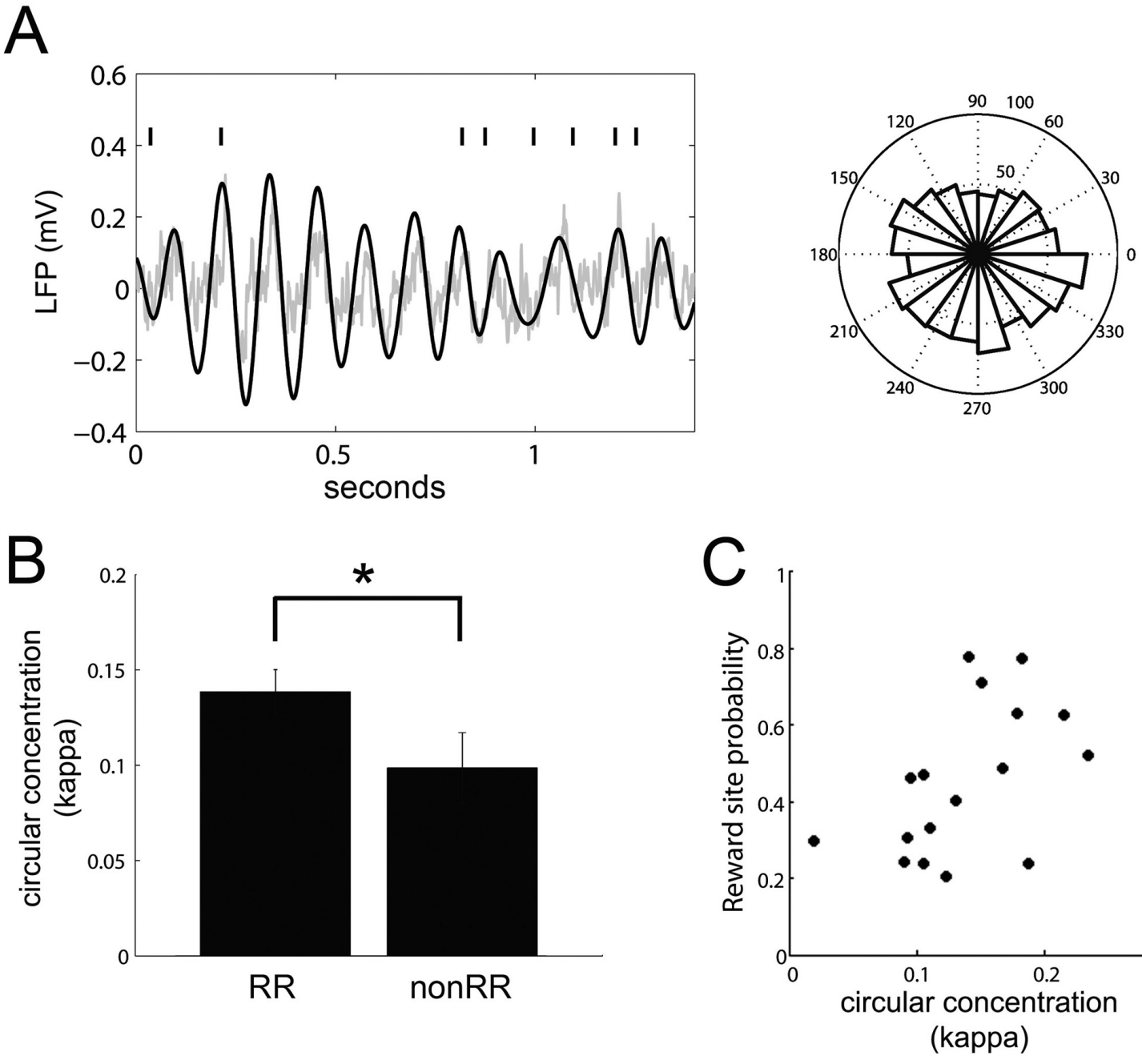
A
0.6
0.4
0.2
0
−0.2
−0.4
LFP (mV)
0
0.5
1
seconds
90
100
60
120
50
30
150
180
0
210
330
240
300
270
B
0.2
0.15
0.1
0.05
0
circular concentration
(kappa)
*
RR
nonRR
C
1
0.8
0.6
0.4
0.2
0
Reward site probability
0
0.1
0.2
0.3
circular concentration
(kappa)

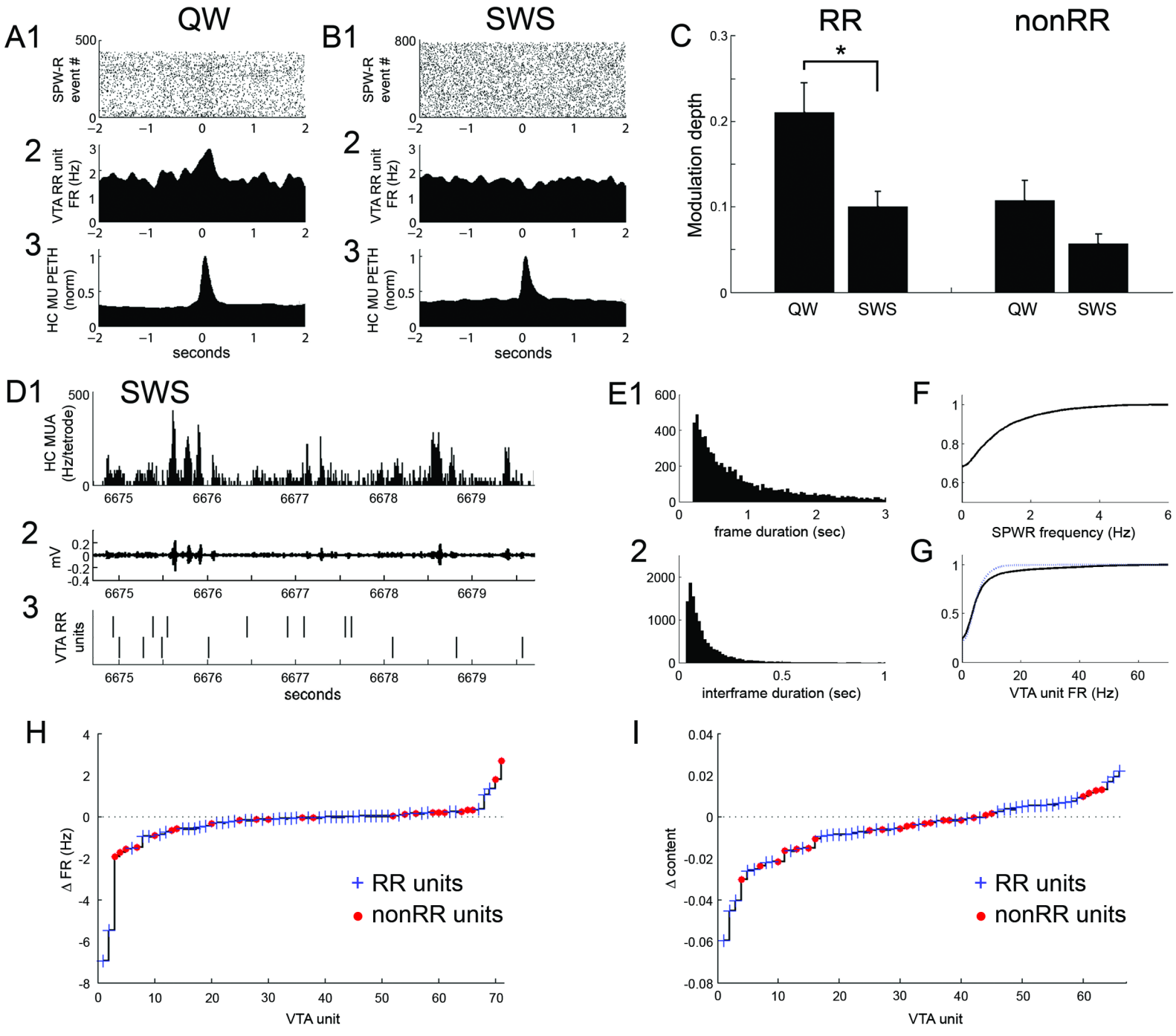
A1
QW
SPW-R event #
VTA RR unit FR (Hz)
HC MU PETH (norm)
seconds
B1
SWS
C
RR
nonRR
Modulation depth
QW
SWS
D1
SWS
HC MUA (Hz/tetrode)
mV
VTA RR units
seconds
E1
frame duration (sec)
interframe duration (sec)
F
SPWR frequency (Hz)
G
VTA unit FR (Hz)
H
Δ FR (Hz)
RR units
nonRR units
VTA unit
I
Δ content
RR units
nonRR units
VTA unit

Bregma: -4.80 mm

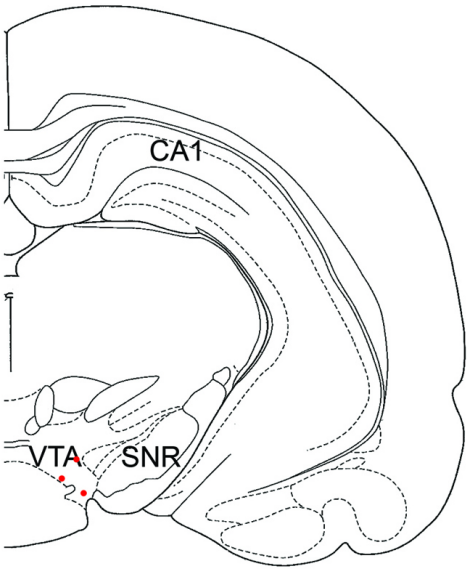

Bregma: -5.30mm

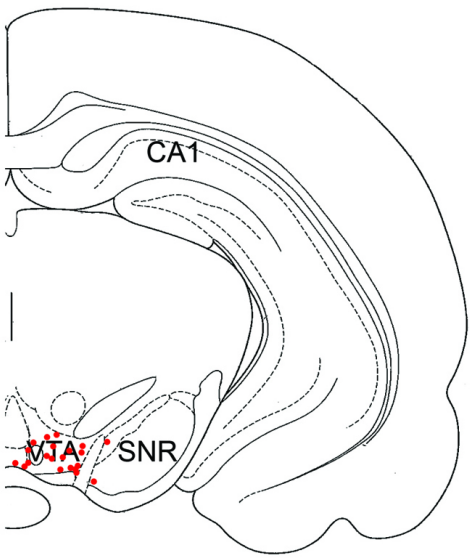

Bregma: -6.04mm